Solution structure of the 40,000 M_r phosphoryl transfer complex between the N-terminal domain of enzyme I and HPr

Daniel S. Garrett[1], Yeong-Jae Seok[2,3], Alan Peterkofsky[2], Angela M. Gronenborn[1] and G. Marius Clore[1]

The solution structure of the first protein-protein complex of the bacterial phosphoenolpyruvate: sugar phosphotransferase system between the N-terminal domain of enzyme I (EIN) and the histidine-containing phosphocarrier protein HPr has been determined by NMR spectroscopy, including the use of residual dipolar couplings that provide long-range structural information. The complex between EIN and HPr is a classical example of surface complementarity, involving an essentially all helical interface, comprising helices 2, 2', 3 and 4 of the α-subdomain of EIN and helices 1 and 2 of HPr, that requires virtually no changes in conformation of the components relative to that in their respective free states. The specificity of the complex is dependent on the correct placement of both van der Waals and electrostatic contacts. The transition state can be formed with minimal changes in overall conformation, and is stabilized in favor of phosphorylated HPr, thereby accounting for the directionality of phosphoryl transfer.

Phosphoryl transfer plays a central role in numerous signal transduction pathways. One such pathway is the phosphoenolpyruvate:sugar phosphotransferase system (PTS) of bacteria which is involved in the coupled phosphorylation and translocation of sugars across the cytoplasmic membrane, chemotaxis towards carbon sources, and the regulation of a number of metabolic pathways[1,2]. Phosphoryl transfer in the PTS involves an associative mechanism in which successive protein–protein complexes between phosphoryl donor and acceptor molecules are formed. The first protein in the PTS pathway is enzyme I (EI) which is autophosphorylated by phosphoenolpyruvate (PEP) at His 189. Phosphorylated EI acts as the phosphoryl donor to His 15 of the histidine-containing phosphocarrier protein, HPr. Phosphorylated HPr in turn donates the phosphoryl group to sugar transporters, collectively known as enzymes II (EII). EI is a 64,000 M_r protein comprising N- and C-terminal domains[3,4]. The N-terminal domain (EIN), which terminates in a linker region extending from Glu 252 to Leu 264, can be phosphorylated in a fully reversible manner by phosphorylated HPr, although it has lost its ability to be autophosphorylated by PEP, a reaction that requires the additional presence of the C-terminal domain[4–6]. Crystal and NMR structures have been reported for EIN[7,8], HPr[9–15] and various EIIs[16–20]. To date, however, no structure of a protein–protein complex of the PTS pathway has been solved. In this paper, we present the solution structure of the 40,000 M_r complex between EIN and HPr, and characterize the interactions that may stabilize the phosphoprotein transition state. To our knowledge this is the first example of a structure of a protein–protein phosphoryl transfer complex.

Structure determination

The EIN–HPr complex is in fast exchange on the chemical shift scale with an equilibrium association constant of ~1.5×10^5 M^{-1} and a lower limit for the dissociation rate constant of ~10^3 s^{-1} (ref. 21). The rotational correlation time of the complex at 40 °C, determined from the distribution of ^{15}N T_1/T_2 ratios[22], is ~15.5 ns with a diffusion anisotropy of ~1.7. The solution structure of the unphosphorylated 1:1 EIN–HPr complex was solved by multidimensional heteronuclear NMR spectroscopy[23], using multiple combinations of isotopically labeled (^{15}N, ^{13}C and/or ^{2}H) proteins to simplify the spectra for assignment purposes and to observe specifically intermolecular nuclear Overhauser (NOE) contacts between EIN and HPr. A total of 30 3D and 8 4D multidimensional NMR spectra were recorded on the 1:1 E1N–HPr complex. In addition, a number of 2D heteronuclear correlation spectra were recorded to check the samples, to measure heteronuclear ^{3}J scalar couplings using quantitative J correlation spectroscopy, and to determine residual dipolar couplings. The total NMR measurement time was ~3,500 h, of which >95% was taken up by the 3D and 4D spectra. An example of the quality of the NMR data is displayed in Fig. 1 which illustrates strips taken from the 3D ^{13}C-separated/^{12}C-filtered NOE spectra recorded on samples of $^{13}C/^{15}N/^{1}H$ EIN:$^{12}C/^{14}N/^{1}H$ HPr and $^{12}C/^{14}N/^{1}H$ EIN:$^{13}C/^{15}N/^{1}H$ HPr. These experiments specifically detect intermolecular NOEs from ^{13}C-attached protons to ^{12}C-attached protons. Other experiments used to identify intermolecular interproton distances comprised ^{15}N-filtered/^{13}C-separated and ^{13}C-filtered/^{15}N-separated NOE experiments using samples in which one component of the complex was labeled with $^{15}N/^{2}H$ and the other with ^{13}C, and 3D ^{15}N-separated NOE experiments in which one of the components was labeled with ^{15}N and ^{2}H. The structure of the complex was calculated by simulated annealing[24] on the basis of 5,474 experimental NMR restraints, including 110 intermolecular NOE-derived interproton distance restraints and 244 one-bond ^{15}N-^{1}H residual dipolar couplings. The latter, which were measured in the nematic phase of a colloidal suspension of *fd* phage[25], supply key long-range structural information for orienting the two proteins relative to

[1]Laboratory of Chemical Physics, Building 5, National Institute of Diabetes and Digestive and Kidney Diseases, National Institutes of Health, Bethesda, MD 20892-0520, USA. [2]Laboratory of Biochemical Genetics, Building 36, National Heart, Lung and Blood Institute, National Institutes of Health, Bethesda, MD 20892, USA. [3]Department of Microbiology, College of Natural Sciences, Seoul National University, Seoul 151-742, Korea.

Correspondence should be addressed to: G.M.C. email: clore@speck.niddk.nih.gov or A.M.G. email: gronenborn @vger.niddk.nih.gov

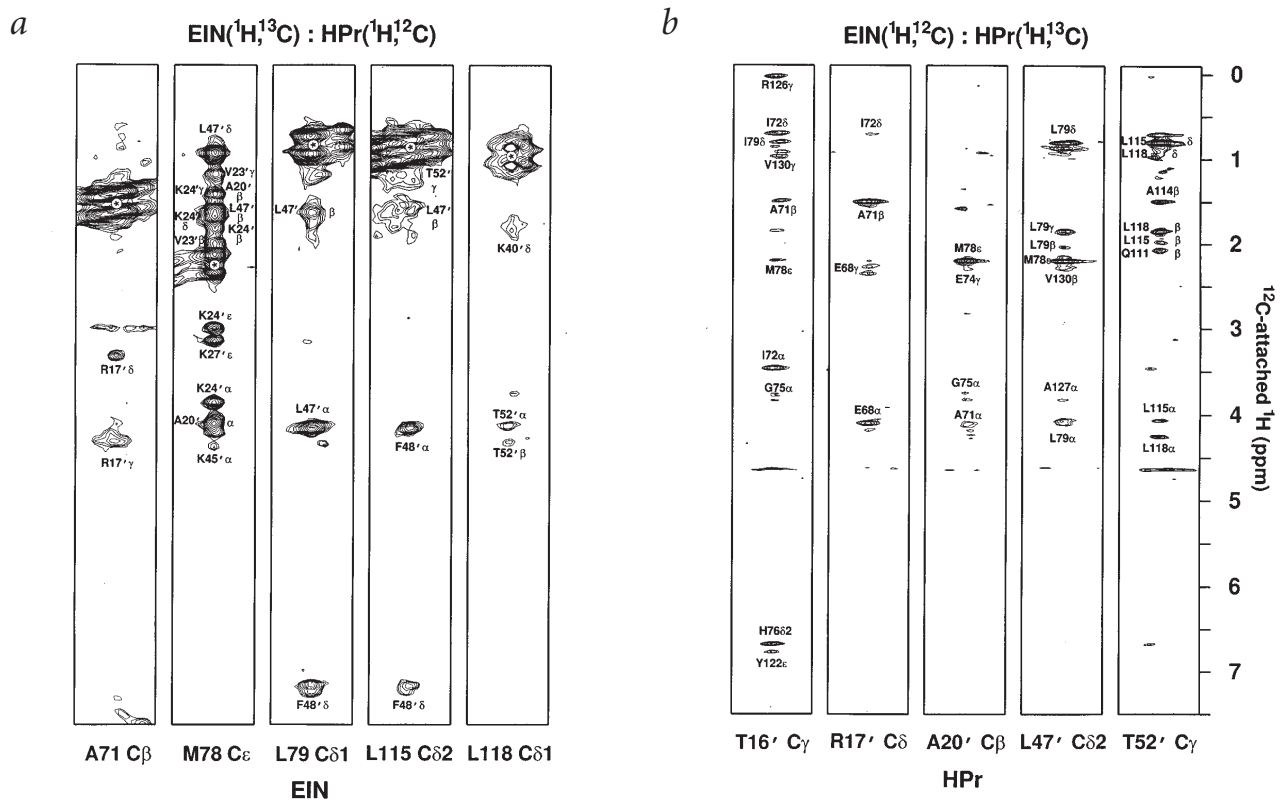

Fig. 1 Strips taken from ***a***, the 3D ^{12}C-filtered(F_1)/^{13}C-separated(F_2) NOE spectrum recorded on a 1:1 ^{15}N/^{13}C/^{1}H EIN:^{14}N/^{12}C/^{1}H HPr complex and ***b***, the 3D ^{13}C-separated(F_2)/^{12}C-filtered(F_3) NOE spectrum recorded on a 1:1 ^{14}N/^{12}C/^{1}H EIN:^{15}N/^{13}C/^{1}H HPr complex, illustrating specifically intermolecular NOE contacts between ^{13}C-attached protons of one component and ^{12}C-attached protons of the other. Residues from HPr are designated by a prime following the residue number. Note that in (*a*) the ^{12}C-attached protons (belonging to HPr) are detected in the indirect dimension (at low digital resolution), hence the broadness of the cross-peaks in the displayed strips; in (*b*) the ^{12}C-attached protons (belonging to EIN) are detected in the acquisition dimension (at high digital resolution) so that the cross-peaks in the displayed strips are narrow..

each other[26]. A summary of the structural statistics is provided in Table 1, and a superposition of the final 40 simulated annealing structures is shown in Fig. 2*a*.

Overall structure of the complex

Two views illustrating the overall complex are shown as ribbon diagrams in Fig. 2*b*. EIN comprises two subdomains: the α domain (residues 33–143), shown in red, is a four helix bundle comprising helices H1, H2/H2', H3 and H4; the α/β domain (residues 1–20 and 148–230), shown in blue, comprises a β-sandwich, formed by a four-stranded parallel β-sheet (β1–β4) and a three-stranded antiparallel β-sheet (β1, β5, β6), as well as three short helices (H5–H7); in addition, there is a long C-terminal helix (H8) that serves as a linker to the C-terminal domain of EI. HPr comprises three helices and a four stranded antiparallel β-sheet. The structures of EIN and HPr in the complex are very similar to those in the free state. The backbone atomic root mean square (r.m.s.) difference between EIN in the complex and the X-ray[7] and NMR[8] structures of free EIN are ~1.2 Å for the α and α/β subdomains combined, and 0.9–1.0 Å for the α and α/β subdomains individually; the backbone atomic r.m.s. differences between HPr in the complex and the X-ray[12] and NMR[13] structures of free *E. coli* HPr are 0.6 and 1.3 Å, respectively. These differences are within the errors of the coordinates.

The interaction between EIN and HPr involves exclusively the α subdomain of EIN, consistent with previous chemical shift perturbation mapping[21]. The long axes of the EIN and HPr molecules are oriented at an angle of ~25° (Fig. 2*b*). The buried surface area at the interface is extensive (944 Å^2 for EIN and 969 Å^2 for HPr) and the interface extends over a region of ~30 Å in length and ~25 Å in width. The interaction surface on EIN comprises virtually the entire helix 2, the N-terminal end of helix 2', the C-terminal half of helix 3 and the N-terminal half of helix 4. The interaction surface on HPr comprises helix 1, helix 2, and the turn preceeding helix 1 and the beginning of the loop following helix 2. Helix 1 of HPr is packed against helices 2 and 4 of EIN at angles of ~55° and ~75°, respectively. Helix 2 of HPr is packed against helices 2, 2', 3 and 4 of EIN at angles of ~110°, 105°, 31° and 150°, respectively.

The EIN–HPr interface

A detailed view of the interface and a summary of the contacts between the two proteins are shown in Fig. 3*a*,*b*. There are 44 residues at the interface, 21 from EIN and 23 from HPr. The majority of the contacts between the two proteins are hydrophobic in nature. Key residues in this regard — that is, those involved in three or more intermolecular contacts — are Ala 71, Ile 72, Met 78, Leu 79, Leu 115, Tyr 122, Leu 123 and Arg 126 of EIN, and Thr 16', Arg 17', Ala 20', Leu 47', Phe 48' and Thr 52' of HPr (the prime is used to designate residues of HPr). In addition, there are 11 intermolecular electrostatic interactions, including two side chain to backbone hydrogen bonds and six

salt bridges. The hydroxyl group of Tyr 122 and the guanidino group of Arg 126 of EIN are hydrogen-bonded to the backbone carbonyl of Leu 14' of HPr. The salt bridges, which were identified using the criteria described by Omichinski *et al.*[27] and represented by six ambiguous $(\Sigma r^{-6})^{-1/6}$ sum distance restraints during the final stages of refinement, comprise the following pairs of EIN and HPr residues: Glu 67 and Arg 17', Glu 68 and Arg 17', Glu 74 and Lys 24', Asp 82 and Lys 27', Glu 84 and Lys 45', and Glu 84 and Lys 49'. In addition, the carboxylate of Asp 82 is not only involved in an intermolecular salt bridge but also accepts two hydrogen bonds from the backbone amides of Glu 84 and Leu 85 which serve to stabilize the kink between helices 2 and 2' of EIN. Finally, there are three side chain–side chain hydrogen bonding interactions between Asp 129 and Thr 16', Glu 84 and Ser 46', and Arg 126 and Gln 51'. It is worth noting that of the 17 residues involved in intermolecular electrostatic interactions, two residues of EIN (Asp 82, Asp 129) and three of HPr (Arg 17', Lys 45' and Ser 46') are conserved throughout all bacterial species. This suggests that these five residues are important for directing the correct alignment of HPr on EI to permit phosphoryl transfer. This notion is supported by the finding that mutation of Asp 129 to Ala or Arg results in loss of EI activity (Y.-J.S. and A.P., unpublished data). Interestingly, phosphorylation of Ser 46' of *Bacillus subtilis* HPr[28] and mutation of Ser 46' to Asp[29] in *Escherichia coli* HPr inhibits the phosphoryl transfer from EI to HPr by two to three orders of magnitude. This effect may possibly be due to destabilization of the EI–HPr complex arising from the close proximity of the negatively charged phosphate of phosphorylated Ser 46' of HPr to the carboxylate of Glu 84 of EIN.

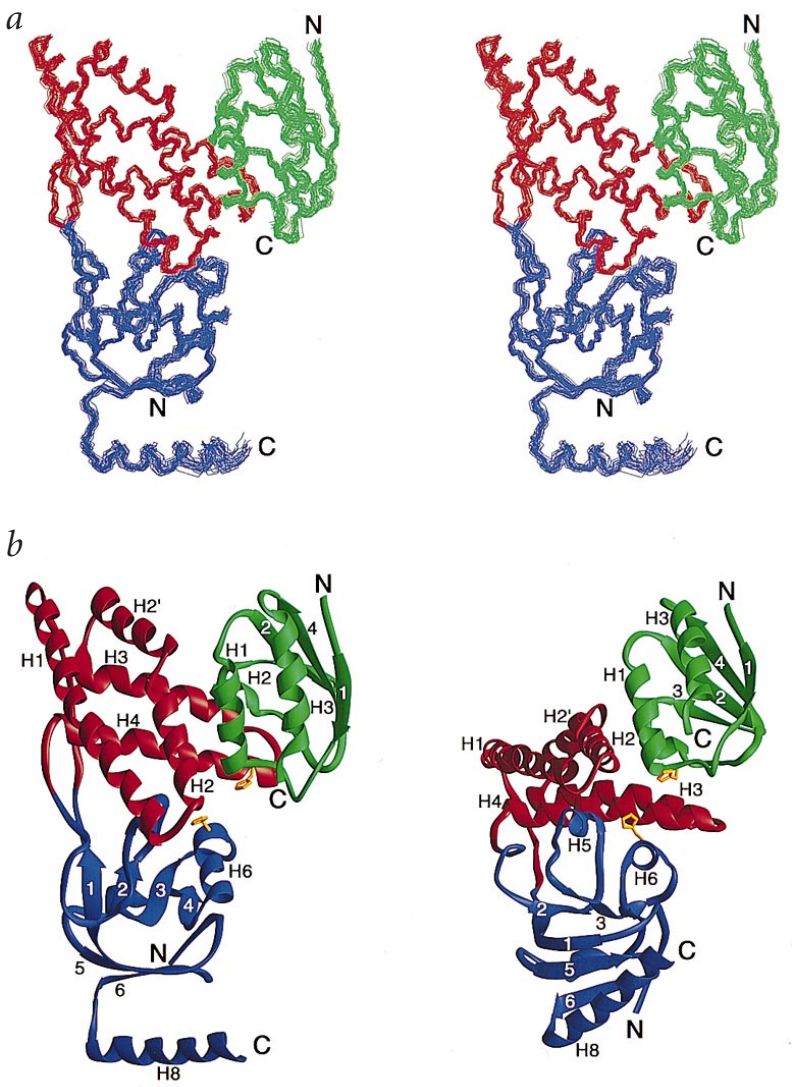

Fig. 2 Structure of the EIN–HPr complex. ***a***, Superposition of the backbone (N, Cα, C atoms) of the 40 simulated annealing structures of the EIN–HPr complex. ***b***, Ribbon diagrams illustrating two views of the EIN–HPr complex. HPr is shown in green, the α domain of EIN in red, and the α/β domain and C-terminal helix of EIN in blue. Also shown in (*b*) in gold are the side chains of His 189 of EIN and His 15' of HPr. Residues 1–250 of EIN and 1–85 of HPr are displayed.

The transition state

EIN and HPr are phosphorylated at the Nε2 atom of His 189[30,31] and the Nδ1 atom of His 15'[14,15,32], respectively. In the unphosphorylated form of the complex, His 189 makes no contacts with HPr, and the Nε2 atom of His 189 accepts a hydrogen bond from the hydroxyl proton of Thr 168, just as it does in free EIN[7,8], so that it is directed away from the Nδ1 atom of His 15' at a distance of ~8.2 Å. Unfortunately, the phosphorylated state of the complex cannot be investigated by NMR since it is not sufficiently stable and long lived. Nevertheless, the present results can be readily used to model the transition state. Isotope labeling experiments have shown that odd and even numbers of phosphoryl transfer steps result in inversion and retention, respectively, of the configuration of the phosphorus[33], consistent with a transition state comprising a pentacoordinated phosphoryl group in a trigonal bipyramidal geometry, with the donor and acceptor atoms in apical positions, and the oxygen atoms lying in the equatorial plane[34]. To model the transition state, we therefore proceeded as follows: we removed the intramolecular NOE between the side chain of His 189 and the methyl group of Thr 168 and the χ_2 restraint of 90 ± 30° for the side chain of His 189; a phosphoryl group was added to the coordinates halfway between His 189 and His 15', and covalent geometry restraints were added for the Nε2(His 189)-P and Nδ1(His 15')-P bonds (set to 2 Å) and the trigonal bipyramidal geometry at the phosphorus. Simulated annealing was then carried out using all the other experimental NMR restraints, and an ensemble of 40 structures was calculated. The precision of the resulting coordinates (~0.5 Å for the backbone) and the agreement with the experimental NMR restraints are the same as that of the EIN–HPr complex in the absence of phosphorus (Table 1), and the overall backbone atomic r.m.s. shift between the two sets of mean coordinates (with and without the phosphorus) is only 0.38 Å, which is well within the precision of the coordinates (Fig. 4*a*). A superposition of the two restrained regularized mean structures comprising helices 5 and 6 of EIN and helix 1 of HPr is shown in Fig. 4*b*, and a detailed view of the active site in the

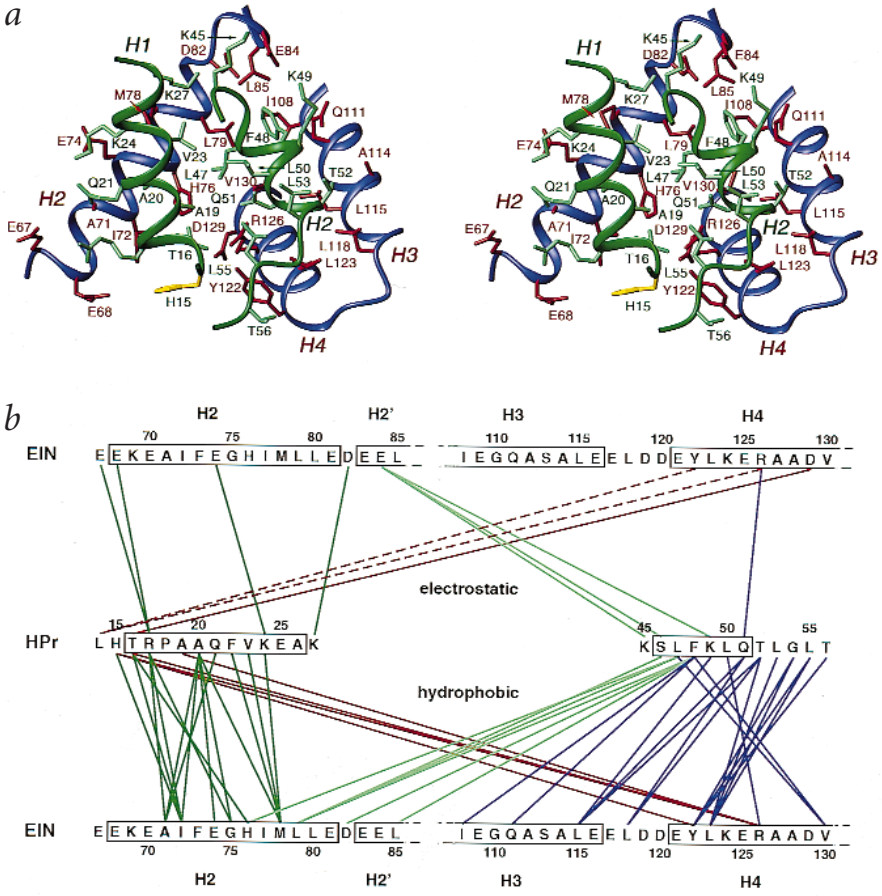

Fig. 3 EIN–HPr interactions. ***a***, Stereo view of the EIN–HPr interface. The backbones of EIN and HPr, depicted as a ribbon diagram, are shown in blue and dark green, respectively; the side chains of EIN and HPr are shown in red and light green, respectively; and His 15' of HPr is shown in gold. Residues of EIN and HPr are labeled in red and green, respectively. ***b***, Summary of electrostatic (top) and van der Waals (bottom) interactions between EIN and HPr. The red lines indicate interactions between helix 1 of HPr and helix 4 of EIN, the green lines between helices 1 and 2 of HPr and helices 2 and 2' of EIN, and the blue lines between helix 2 of HPr and helices 3 and 4 of EIN. The dashed red lines for the electrostatic interactions represent side chain–backbone hydrogen bonds.

putative transition state is depicted in Fig. 4*c*. The only significant structural change required to form the transition state involves the χ_2 side chain conformation of His 189 which flips ~120° from the g^+ to the g^- rotamer, thereby permitting the Nε2 atom of His 189 to come into close proximity (4 Å) to the Nδ1 atom of His 15' (Fig. 4*b*). This is accompanied by a concerted lateral rigid body displacement of helices 5 and 6 in opposite directions resulting in a small increase of ~1 Å in their interhelical separation, which can be attributed to a combination of steric clash between the Cε1-Hε1 group of His 189 and the Oγ1 atom of Thr 168 and the pulling effect on helix 6 exerted by the linear arrangement of the Nε2(His 189)-P-Nδ1(His 15) atoms with a 4 Å separation between the two nitrogen atoms (Fig. 4*b*). The χ1 angle of His 189 and the χ1/χ2 of His 15 remain in the same rotamer, albeit with changes in torsion angle values of 10–20°. Thus the χ1/χ2 side chain torsion angles of His 189 and His 15 change from 179 ± 5°/81 ± 6° and 74 ± 3°/115 ± 6°, respectively, in the unphosphorylated complex to -157 ± 1°/-70 ± 4° and 59 ± 2°/136 ± 2°, respectively, in the transition state. In addition, there are some very minor (5–10°) changes in the backbone ϕ/ψ torsion angle of His 189 and His 15 to accommodate the pentacoordinate phosphorus.

The pentacoordinate phosphorus in the transition state is located at the bottom of a cleft formed by the N-terminal end of helix 2 of EIN, helix 6 of EIN and the N-terminal end of helix 1 of HPr (Fig. 4*a*,*c*). A number of electrostatic interactions stabilize the transition state (Fig. 4*c*). Arg 17' of HPr, which is known to be a crucial residue for phosphoryl transfer[1,35], neutralizes the negative charges arising from Glu 67 and Glu 68 of EIN which lie in close proximity to the phosphorus (Fig. 4*c*). In addition, there are electrostatic interactions between Lys 69 of EIN and the phosphate, and hydrogen bonds from the backbone amide groups of Thr 16' and Arg 17' and the hydroxyl group of Thr 16' of HPr to the phosphate. The latter three hydrogen bonds are also observed in the uncomplexed form of phosphorylated HPr[14,15]. Thus, from a structural perspective, the transition state is stabilized in favor of phosphorylated HPr relative to phosphorylated EIN. In addition, phosphorylation of EIN destabilizes EIN, reducing its melting temperature by ~6 °C[36], presumably in part due to the loss of the hydrogen bond between His 189 and Thr 168, which would also favor phosphoryl transfer from EIN to HPr. Both factors could be important in stimulating the appropriate phosphotransfer flow in the PTS.

Specificity of phosphotransfer

Although the sequence similarity among the various EIs and HPrs is high, there is considerable specificity in the EI–HPr interaction. The rate of cross-phosphotransfer from EI to HPr between the EIs and HPrs from *E. coli* and *B. subtilis* is ~5% that of the homologous reactions[37]. Further, the rate of phosphotransfer from *E. coli* EI to *Mycoplasma capricolum* HPr is only 10% of that using *E. coli* HPr[38]. Removal of the C-terminal domain of EI results in a relaxation of this species specificity[5]. Consequently, the contribution of the individual intermolecular contacts observed in the EIN–HPr complex to the interaction of intact EI with HPr as well as to the species specificity can be evaluated.

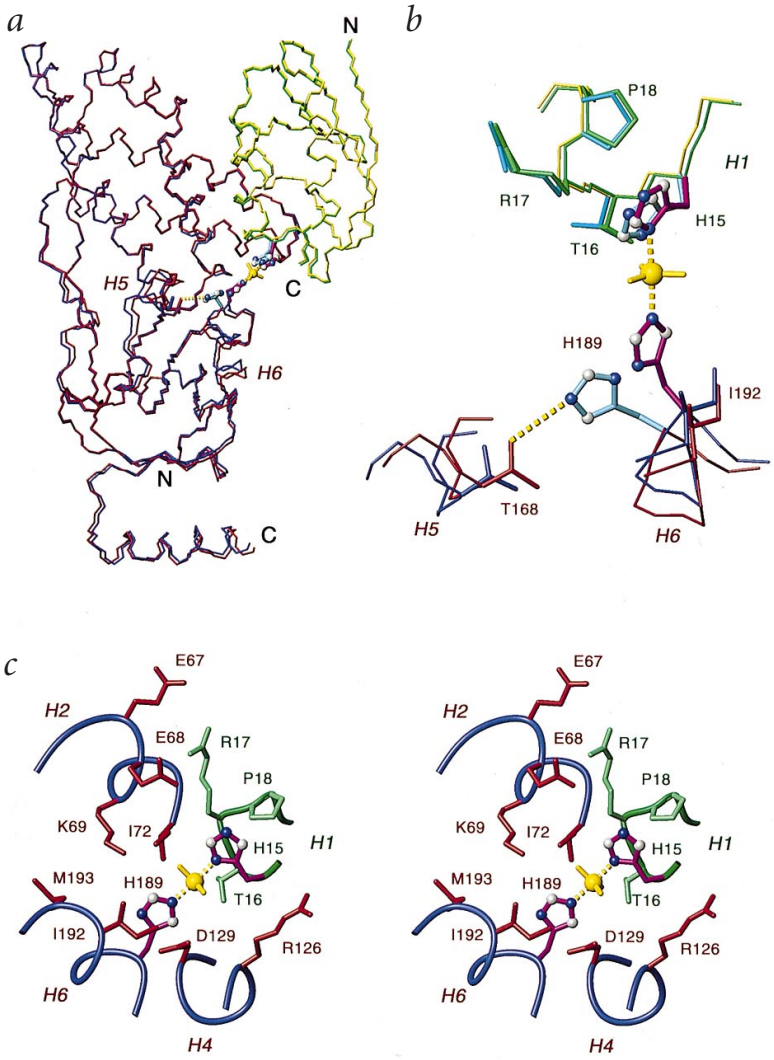

Fig. 4 The transition state. ***a***, Overall superposition of the backbone coordinates of the unphosphorylated EIN–HPr complex and the transition state. ***b***, Detailed view showing a superposition of helices 5 and 6 of EIN and helix 1 of HPr in the unphosphorylated EIN–HPr complex and in the transition state, illustrating the change in conformation of His 189 of EIN and His 15' of HPr, and the lateral displacement of helices 5 and 6 of EIN. ***c***, Detailed view of the active site illustrating the putative transition state. The phosphorus atom in the transition state is pentacoordinate with trigonal bypyramidal geometry; the Nε2 atom of His 189 of EIN and Nδ1 atom of His 15 of HPr are located in apical positions and separated by 4 Å, while the three oxygen atoms lie in the equatorial plane. The color coding is as follows. In (*a*) and (*b*) the backbone of EIN and HPr are shown in red and yellow, respectively, in the unphosphorylated complex, and in blue and green, respectively, in the transition state; His 189 and His 15 are shown in light blue in the unphosphorylated complex and in purple in the transition state with the ring nitrogens of His 189 and His 15 represented as blue balls, and the ring carbons of His 189 and His 15 as grey balls; the phosphoryl group is shown in yellow. In (*c*), the backbones of EIN and HPr, displayed as tubes, are shown in blue and dark green, respectively; the side chains of EIN and HPr are shown in red and light green, respectively; and the phosphoryl group is shown in yellow. Residues of EIN and HPr are labeled in red and green, respectively.

An alignment of the sequences of the HPrs and EIs from *E. coli*, *B. subtilis* and *M. capricolum* in the regions involved in the *E. coli* HPr–EIN interaction (Fig. 5) shows several conserved residues (shaded in red). A number of residues are absolutely conserved in the three species. This includes residues directly involved in the EIN–HPr interface (His 15', Arg 17', Lys 45', Ser 46' for HPr; Ile 72, His 76, Asp 82, Tyr 122, Arg 126 and Asp 129 for EIN). In addition, there are residues (Gly 13', Pro 18' and Ala 26' for HPr; Gly 66, Lys 69, Phe 73, Lys 125, Glu 125 and Ala 128 for EIN) that are conserved but not directly involved in the EIN–HPr interface. Gly 13' and Ala 26' of HPr and Gly 66 and Phe 73 of EIN play a structural role: the two glycine residues are located in turns, and the other two residues are internal hydrophobic residues. Pro 18' of HPr packs directly against His 15' and is presumably important in stabilizing the orientation of His 15' for optimal phoshoryl transfer. Lys 69 of EIN is important for stabilizing the phosphoryl group both in phosphorylated EIN and in the EIN–HPr phosphoryl transition state complex (Fig. 4*c*). Lys 124, Glu 125 and Ala 128 of EIN form a contiguous patch on the surface of helix 4 facing away from the interface with HPr. It is conceivable that these residues are necessary for the autophosphorylation activity of EI.

Many residues involved in the EIN-HPr interface are subject to conservative substitutions in the three species (Leu 14', Thr 16', Ala 20', Phe 22', Val 23', Leu 47' Phe 48', Leu 50', Thr 52', Leu 53', Gly 54' and Leu 55' of HPr, and Glu 67, Glu 68, Gly 75, Leu 79, Leu 85 Ala 112, Leu 115, Leu 118, Leu 123 and Val 130), supporting the importance of these residues for the binding of HPr to EIN. In contrast, there are some residues (Gln 21', Lys 24', Lys 27', Lys 49', Gln 51' and Thr 56' of HPr and Ala 71, Glu 74, Met 78, Glu 84, Ile 108 and Gln 111 of EIN) that participate in the EIN–HPr interactions but are not well conserved throughout the three species. In some cases, the non-conservative substitution is likely to improve the stability of the complex; such as is the case, for example, with the substitution of Gln 21' by Val, and of Gln 111 by Phe or Tyr which would be predicted to increase the strength of the hydrophobic interactions at the interface. In other cases the substitution is likely to decrease the stability of the complex through loss of either a hydrophobic (for example, Ile 108 to Ser) or electrostatic (for example, Lys 27' to Ser) contact. Finally other substitutions are likely to have a neutral effect; for example, the substitution of Gln 51' by Met will remove the electrostatic interaction with Arg 126 but will enhance the hydrophobic interactions with Leu/Phe/Tyr 115, Leu/Met 118 and Arg 126.

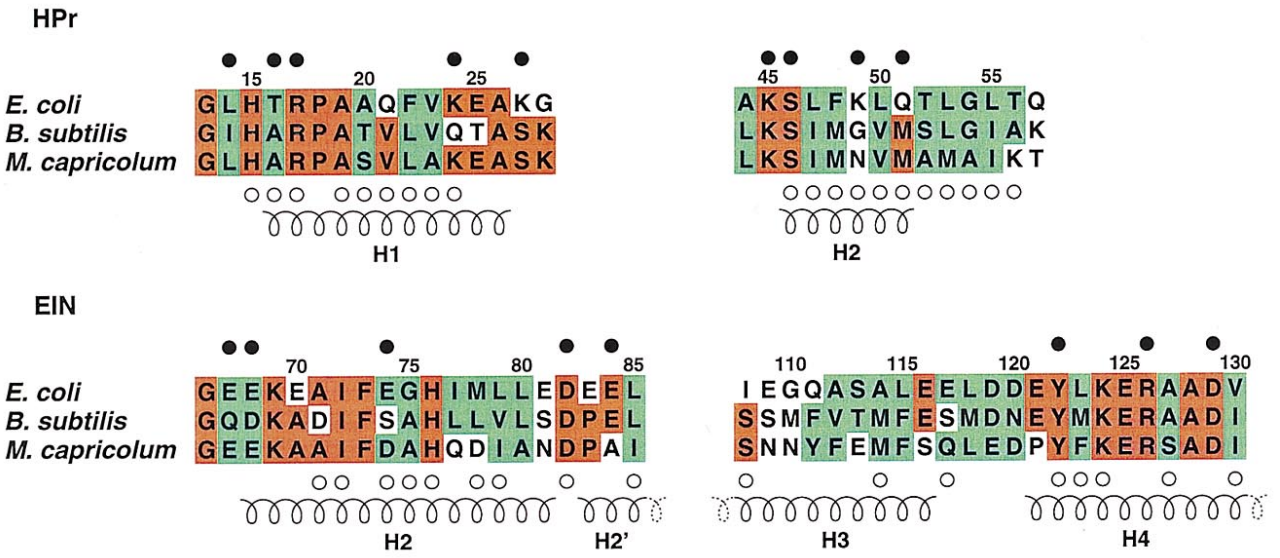

Fig. 5 Sequence comparison of HPrs and EIs from *E. coli*, *B. subtilis* and *M. capricolum* around the regions associated with the EIN–HPr interface. Residues shaded in red are conserved and in green are conservatively substituted. The sequence numbering corresponds to that of the *E.coli* proteins. The filled-in (above the sequences) and open (below the sequences) circles designate residues involved in electrostatic and hydrophobic interactions, respectively, at the EIN–HPr interface.

The analysis of the electrostatic interactions (Fig. 3*b*), together with the sequence alignments (Fig. 5), may provide insight into the specificity for phosphotransfer from EI to HPr observed in intact *E. coli* EI which is relaxed in *E. coli* EIN[5]. Thr 16' of *E. coli* HPr is replaced by Ala in both *M. capricolum* and *B. subtilis*[39], resulting in loss of both the Asp 129–Thr 16' interaction, as well as the postulated hydrogen bond between the hydroxyl of Thr 16' and the phosphoryl group in the transition state. The Asp 82–Lys 27' interaction is eliminated by conversion to Ser 27'. The same holds true for the Glu 84–Lys 49' salt bridge when Lys 49' is converted to Gly 49' or Asn 49'. In the absence of the C-terminal domain of *E. coli* EI, these interactions are apparently dispensable. However, with intact *E. coli* EI, they may be essential and responsible for the observed species specificity with the full-length *E. coli* protein.

Finally, the side chain–backbone hydrogen bonds involving Arg 126 and Tyr 122 of EIN and Leu(Ile) 14' of HPr, and the salt bridges between Glu(Gln) 67 and Glu(Asp) 68 of EIN and Arg 17' of HPr are essentially conserved in all three species and are likely to be crucial for phosphotransfer activity.

In summary, the structure of the EIN–HPr complex has delineated the specific electrostatic and hydrophobic interactions at the intermolecular interface and has permitted the evaluation of critical specificity features of the first protein–protein interaction of the PTS.

Methods

Sample preparation. EIN (1–258 + Arg) and HPr were expressed, purified and isotopically labeled with ^{15}N (>95%), ^{13}C (>95%) and ^{2}H (>85%) as described previously[8,21]. Samples for NMR contained ~1 mM 1:1 EIN–HPr complex in 10 mM phosphate buffer pH 7.0. The following samples were employed (only the presence of ^{2}H, ^{15}N and ^{13}C isotopes are indicated; if no H, C or N isotope is mentioned, then the sample contained ^{1}H, ^{12}C or ^{14}N at natural isotopic abundance): EIN(^{2}H,^{15}N):HPr, EIN(^{15}N):HPr, EIN(^{2}H,^{13}C,^{15}N):HPr, EIN(^{13}C,^{15}N):HPr, EIN: HPr(^{2}H,^{15}N), EIN:HPr(^{15}N), EIN:HPr(^{2}H,^{13}C,^{15}N), EIN:HPr(^{13}C,^{15}N), EIN(^{2}H,^{15}N): HPr(^{13}C), EIN(^{13}C):HPr(^{2}H,^{15}N), EIN(^{13}C,^{15}N):HPr(^{2}H,^{15}N), EIN(^{2}H,^{15}N):HPr(^{13}C,^{15}N), EIN(^{2}H,^{15}N):HPr(^{2}H,^{15}N), and EIN(^{13}C,^{15}N):HPr(^{13}C,^{15}N).

NMR spectroscopy. All spectra were recorded at 40 °C on Bruker DMX600 and DMX750 spectrometers. ^{1}H, ^{15}N and ^{13}C sequential assignments were obtained using 3D double and triple resonance through-bond correlation experiments on both protonated and perdeuterated samples; ^{3}J couplings were measured using quantitative 2D and 3D J correlation spectroscopy; interproton distance restraints were derived from multidimensional NOE spectra with mixing times ranging from 50 to 75 ms[23]. 3D experiments used for sequential assignments included HNCO, HNHA, HNCA, HNCACB, CBCA(CO)NH, C(CCO)NH, d-HNCACB, d-CBCA(CO)NH, d-C(CCO)NH, HBHA(CBCACO)NH, H(CCO)NH, HCCH-COSY and HCCH-TOCSY as described in the structure determination of free EIN[8]. NOE experiments included 3D ^{13}C-separated, ^{15}N-separated, ^{13}C-separated/^{12}C-filtered, ^{13}C-separated/^{15}N-filtered and ^{15}N-separated/^{13}C-filtered NOE spectra, 4D $^{13}C/^{15}N$-separated, $^{15}N/^{15}N$-separated and $^{13}C/^{13}C$-separated NOE spectra. Residual $^{1}D_{NH}$ dipolar couplings were obtained by taking the difference in the corresponding J splittings measured in oriented (in ~23 mg ml^{-1} colloidal suspension of *fd* phage[25]) and isotropic (in water) EIN:HPr complex ($^{15}N/^{2}H$ labeled) using 2D IPAP {^{15}N,^{1}H}-HSQC experiments[40]. The precision of the measured $^{1}D_{NH}$ couplings was ~0.5–1.0 Hz. The magnitude of the axial (-14.3 Hz) and rhombic (0.4) components of the alignment tensor D^{NH} was obtained by examining the powder pattern distribution of dipolar couplings[41].

Structure calculations. NOE derived interproton distance restraints were classified into four ranges: 1.8–2.7 Å (1.8–2.9 Å for NOE involving an NH), 1.8–3.3 Å (1.8–3.5 Å for NOE involving an NH), 1.8–5.0 Å and 1.8–6.0 Å corresponding to strong, medium, weak and very weak NOEs; an additional 0.5 Å was added to the upper bound for NOEs involving methyl groups, and distances involving non-stereospecifically assigned protons were represented by a $(\Sigma r^{-6})^{-1/6}$ sum[42]. Hydrogen bonding restraints (two per hydrogen bond where $r_{NH\text{-}O}$ = 1.5–2.8 Å and $r_{N\text{-}O}$ = 2.4–3.5 Å) were deduced from NH exchange experiments, backbone NOEs, and backbone chemical shifts using standard criteria. ϕ and ψ torsion angle restraints were derived from $^{3}J_{HN\alpha}$ coupling constants and a database analysis of backbone (N, HN, Cα, Cβ, C', Hα) chemical shifts using the program TALOS (G. Cornilescu, F. Delaglio

Table 1 Structural statistics[1]

	<SA>	$\overline{(SA)}$r
R.m.s. deviations from interproton distance restraints (Å)[2]		
Intramolecular (2,284/889)	0.038 ± 0.001	0.038
Intermolecular (110)	0.084 ± 0.005	0.086
R.m.s. deviations from intramolecular hydrogen bond restraints (Å) (236/68)[2]	0.033 ± 0.003	0.039
R.m.s. deviation from intermolecular salt bridge restraints (Å) (6)[3]	0.028 ± 0.026	0
R.m.s. deviations from dihedral restraints (°) (768/170)[2]	0.161 ± 0.066	0.128
R.m.s. deviations from $^3J_{HN\alpha}$ coupling constants (Hz) (-/34)[2]	1.00 ± 0.04	1.08
R.m.s. deviations from secondary $^{13}C\alpha$,$^{13}C\beta$ shifts (p.p.m.) (503/162)	1.14 ± 0.01	1.13
R-factor for residual dipolar coupling restraints (%) (165/79)[4]	3.3 ± 0.1	3.3
Deviations from idealized covalent geometry		
bonds (Å) (4 045/1 300)	0.003 ± 0.000	0.005
angles (deg.) (7373/2 363)	0.489 ± 0.007	0.595
impropers (deg.) (1 954/635)	0.566 ± 0.015	0.618
Measures of structure quality		
E_{LJ} (kcal mol^{-1})[5]	-1,496 ± 17	-1,425
PROCHECK[6]		
Residues in most favourable region of Ramachandran plot	89.7 ± 0.9	89.8
No. of bad contacts per 100 residues	5.6 ± 0.9	4.8
Coordinate precision (Å)[7]		
backbone (N, Cα, C', O)	0.55 ± 0.07	
All non-hydrogen atoms	0.84 ± 0.05	

[1]The notation of the NMR structures is as follows: <SA> are the final 40 simulated annealing structures; $\overline{SA}$ is the mean structure obtained by averaging the coordinates of the individual SA structures best-fitted to each other (residues 1-250 of EIN and 1-85 of HPr); $\overline{(SA)}$r is the restrained regularized mean structure obatined by restrained regularization of the mean structure $\overline{SA}$. The number of terms for the various restraints is given in parentheses (the first and second numbers refer to EIN and HPr, respectively).
[2]None of the structures exhibited interproton distance violations >0.5 Å, dihedral angle violations >3°, or $^3J_{HN\alpha}$ coupling constant violations >2 Hz. The intramolecular NOE derived interproton distance restraints comprise the following interresidue sequential (|i - j| = 1), medium range (1 < |i - j| < 5) and long range (|i - j| > 5) NOEs and intraresidue NOEs: 746, 517, 537 and 486, respectively, for EIN; and 274, 167, 246 and 202, respectively, for HPr. Protein backbone hydrogen bonding restraints (two per hydrogen bond, $r_{NH\text{-}O}$ = 1.5–2.8 Å, $r_{N\text{-}O}$ = 2.4–3.5 Å) were introduced during the final stages of refinement according to standard criteria. It should be noted that the torsion angle restraints serve principally to aid convergence of the simulated annealing protocol since, in general, the torsion angles for the ensemble of simulated annealing structures lie well within the error bounds of the torsion angle restraints.
[3]Six ambiguous distance restraints, represented by $(\Sigma r^{-6})^{-1/6}$ sums, were added during the final stages of refinement for salt bridges identified using the criteria described in ref. 27.
[4]The R-factor for the residual dipolar couplings is defined as the ratio of the r.m.s. deviation between observed and calculated values to the expected r.m.s. deviation if the vectors were randomly oriented. The latter is given by $\{2D_a^2[4+3R^2]/5\}^{1/2}$ and for an infinite number of measurements is exactly equal to $(2\Sigma D_{obs}^2)^{1/2}$, where D_a is the magnitude of the axial component of the alignment tensor, R the rhombicity, and D_{obs}, the observed values of the dipolar couplings[25]. The values of D_a and R for the one-bond ^{15}N-^1H dipolar couplings, obtained directly from the powder pattern distribution of the measured dipolar couplings[41], are -14.3 Hz and 0.4, respectively.
[5]The Lennard-Jones van der Waals energy was calculated with the CHARMM PARAM19/20 parameters and is not included in the target function for simulated annealing or restrained regularization.
[6]The overall quality of the structure was assessed using the program PROCHECK[46]. There were no φ/ψ angles in the disallowed region of the Ramachandran plot. The dihedral angle G-factors for φ/ψ, χ_1/χ_2, χ_1, χ_3/χ_4 are 0.08 ± 0.03, 0.59 ± 0.04, 0.18 ± 0.07 and -0.01 ± 0.07, respectively. The conformational database potential does not affect the precision of the resulting ensemble of structures but serves to bias sampling during simulated annealing refinement to conformations that are likely to be energetically possible by effectively limiting the choices of dihedral angles to those that are known to be physically realizable[47].
[7]Defined as average r.m.s. difference (residues 1–250 of EIN and 1–85 of HPr) between the final 40 simulated annealing structures and the mean coordinates. Residues 251–259 of EIN are disordered in solution.

and A. Bax, pers. comm.), which is based on a data base of residue triplets correlating φ,ψ angles (determined from high resolution X-ray structures) and their corresponding backbone secondary shifts. χ_1 and χ_2 torsion angle restraints were derived from analysis of heteronuclear $^3J_{CC}$, $^3J_{NC\gamma}$ and $^3J_{COC\gamma}$ couplings and NOE/ROE experiments[23]. Structures were calculated by simulated annealing[24] using the program CNS[43]. The final values for the force constants employed for the various terms in the target function employed for simulated annealing are as follows: 1000 kcal mol^{-1} Å^{-2} for bond lengths, 500 kcal mol^{-1} rad^{-2} for angles and improper torsions (which serve to maintain planarity and chirality), 4 kcal mol^{-1} Å^{-4} for the quartic van der Waals repulsion term (with the van der Waals radii set to 0.8 times their value used in the CHARMM PARAM19/20 parameters), 30 kcal mol^{-1} Å^{-2} for the experimental distance restraints (interproton distances and hydrogen bonds), 200 kcal mol^{-1} rad^{-2} for the torsion angle restraints, 1 kcal mol^{-1} Hz^{-2} for the $^3J_{HN\alpha}$ coupling constant restraints, 0.5 kcal mol^{-1} p.p.m.$^{-2}$ for the secondary ^{13}C chemical shift restraints, 1.0 kcal mol^{-1} Hz^{-2} for the $^1D_{NH}$ dipolar coupling restraints, and 1.0 for the conformational database potential[42]. Figures were generated using MOLMOL[44] and RIBBONS[45].

Coordinates. Coordinates for the final 40 simulated annealing structures, the corresponding restrained regularized mean structure, and the restrained regularized mean structure of the putative transition state, together with a complete list of experimental NMR restraints have been deposited in the Protein Data Bank (accession codes 3EZA, 3EZB, 3EZC, 3EZD, R3EZAMR).

Acknowledgments
This work was supported in part by the AIDS Targeted Antiviral Program of the Office of the Director of the National Institutes of Health (to G.M.C. and A.M.G.). We thank R. Tschudin for technical hardware support; G. Cornilescu, F. Delaglio and A. Bax for the use of the program TALOS; J. Louis for preparation of *fd* phage; and A. Bax, M. Starich and N. Tjandra for useful discussions.

Received 1 October, 1998; accepted 10 November, 1998.

1. Postma, P.W., Lengeler, J.W. & Jacobson, G.R. Phosphoenolpyruvate:carbohydrate phosphotransferase systems. In *Escherichia coli and Salmonella: Cellular and Molecular Biology* (ed. Neidhardt F.C.) 1149–1174 (ASM Press, Washington DC; 1996).
2. Herzberg, O & Klevit R. Unraveling a bacterial hexose transport pathway. *Curr. Opin. Struct. Biol.* **4**, 814–822 (1994).
3. Licalsi, C., Crocenzi, T.S., Freire, E. & Roseman, S. Sugar transport by the bacterial phosphotransferase system: structural and thermodynamic domains of Enzyme I of *Salmonella typhimurium*. *J. Biol. Chem.* **266**, 19519–19527 (1991).
4. Lee, B.R., Lecchi, P., Pannell, L., Jaffe, H. & Peterkofsky, A. Identification of the N-terminal domain of Enzyme I of the *Escherichia coli* phosphoenolpyruvate:sugar phosphotransfease system produced by proteolytic digestion. *Arch. Biochem. Biophys.* **312**, 121–124 (1994).
5. Seok, Y.-J., Lee, B.R., Zhu, P.-P. & Peterkofsky, A. Importance of the carboxyl terminal domain of Enzyme I of the *Escherichia coli* phosphoenolpyruvate:sugar phosphotransferase system for phosphoryl donor specificity. *Proc. Natl. Acad. Sci. USA* **93**, 347–351 (1996).
6. Chauvin, F., Fomenkov, A., Johnson, C.R. & Roseman, S. The N-terminal domain of *Escherichia coli* enzyme I of the phosphoenolpyruvate/glycose phosphotransferase system: molecular cloning and characterization. *Proc. Natl. Acad. Sci. USA* **93**, 7028–7031 (1996).
7. Liao, D.-I. *et al.* The first step in sugar transport: crystal structure of the amino terminal domain of enzyme I of the *E coli* PEP:sugar phosphotransferase system and a model of the phosphotransfer complex with HPr. *Structure* **4**, 861–872 (1996).
8. Garrett, D.S. *et al.* Solution structure of the 30 kDa N-terminal domain of Enzyme I of the *Escherichia coli* phosphoenolpyruvate:sugar phosphotransferase system by multidimensional NMR. *Biochemistry* **36**, 2517–2530 (1997).
9. Wittekind, M. *et al.* Solution structure of the phosphocarrier protein HPr from Bacillus subtilis by two-dimensional NMR spectroscopy. *Prot. Sci.* **1**, 1363–1376 (1992).
10. Herzberg, O. *et al.* Structure of the histidine-containing phosphocarrier protein HPr from Bacillus subtilis at 2.0 Å resolution. P*roc. Natl. Acad. Sci. USA* **89**, 2499–2503 (1992).
11. Kalbitzer, H.R. & Henstenberg, W. The solution structure of the histidine-containing protein (HPr) from *Staphylococcus aureus* as determined by two-dimensional 1H-NMR spectroscopy. *Eur. J. Biochem.* **216**, 205–214 (1993).
12. Jia, Z., Quail, J.W., Waygood, E.B. & Delbaere, L.T. The 2.0 Å resolution structure of the *Escherichia coli* histidine-containing phosphocarrier protein HPr: a redetermination. *J. Biol. Chem.* **268**, 22490–22501 (1993).
13. van Nuland, N.A. *et al.* The high-resolution structure of the histidine-containing phosphocarrier protein HPr from *Escherichia coli* determined by restrained molecular dynamics from nuclear magnetic resonance nuclear Overhauser effect data. *J. Mol. Biol.* **237**, 544–559 (1994).
14. van Nuland, N.A.J., Boelens, R., Scheek, R.M. & Robillard, G.T. High-resolution structure of the phosphorylated form of the histidine-containing phosphocarrier protein HPr from *Escherichia coli* determined by restrained molecular dynamics from NMR-NOE data. *J. Mol. Biol.* **246**, 180–193 (1995).
15. Jones, B.E., Rajgopal, P. & Klevit, R.E. Phosphorylation on histidine is accompanied by localized structural changes in phosphocarrier protein HPr from *Bacillus subtilis*. *Prot. Sci.* **6**, 2107–2119 (1997).
16. Liao, D.-I. *et al.* Structure of the IIA domain of the glucose permease of *Bacillus subtilis* at 2.2 Å resolution. *Biochemistry* **30**, 9583–9594 (1991).
17. Worthylake, D. *et al.* Three-dimensional structure of the Escherichia coli phosphocarrier protein III^{glc}. *Proc. Natl. Acad. Sci. USA* **88**, 10382–10386 (1991).
18. Fairbrother, W.J., Gippert, G.P., Reizer, J., Saier, M.H. & Wright, P.E. Low resolution structure of Bacillus subtilis glucose pemease IIA derived from heteronuclear three-dimensional NMR spectroscopy. *FEBS Lett.* **296**, 148–152 (1992).
19. Hurley, J.H. *et al.* Structure of the regulatory complex of *Escherichia coli* III^{glc} with glycerol kinase. *Science* **259**, 673–677 (1993).
20. Huang, K., Kapadia, G., Zhu, P.-P., Peterkofsky, A. & Herzberg, O. A promiscuous binding surface: crystal structure of the IIA domain of the glucose-specific permease from Mycoplasma capricolum. *Structure* **6**, 697–710 (1998).
21. Garrett, D.S., Seok,Y.-J., Peterkoksky, A., Clore, G.M. & Gronenborn, A.M. Identification by NMR of the binding surface for the histidine-containing phosphocarrier protein HPr on the N-terminal domain of Enzyme I of the *Escherichia coli* phosphotransferase system. *Biochemistry* **36**, 4393–4398 (1997).
22. Clore, G.M., Gronenborn, A.M., Szabo, A. & Tjandra, N. Determining the magnitude of the fully asymmetric diffusion tensor from heteronuclear relaxation data in the absence of structural information. *J. Am. Chem. Soc.* **120**, 4889–4890 (1998).
23. Clore, G.M. & Gronenborn, A.M. Determining structures of large proteins and protein complexes by NMR. *Trends Biotech.* **16**, 22–34 (1998).
24. Nilges, M., Gronenborn, A.M., Brünger, A.T. & Clore, G.M. Determination of three-dimensional structures of proteins by simulated annealing with interproton distance restraints: application to crambin, potato carboxypeptidase inhibitor and barley serine proteinase inhibitor 2. *Prot. Engng.* **2**, 27–38 (1988).
25. Clore, G.M., Starich, M.R. & Gronenborn, A.M. Measurement of residual dipolar couplings of macromolecules aligned in the nematic phase of a colloidal suspension of rod-shaped viruses. *J. Am. Chem. Soc.* **120**, 10571–10572.
26. Tjandra, N., Omichinski, J.G., Gronenborn, A.M., Clore, G.M. & Bax, A. Use of dipolar ^{1}H-^{15}N and ^{1}H-^{13}C couplings in the structure determination of magnetically oriented macromolecules in solution. *Nature Struct. Biol.* **4**, 732–738 (1997).
27. Omichinski, J.G., Pedone, P.V., Felsenfeld, G., Gronenborn, A.M. & Clore, G.M. The solution structure of a specific GAGA factor-DNA complex reveals a modular binding mode. *Nature Struct. Biol.* **4**, 122–132 (1997).
28. Reizer, J. *et al.* Mechanistic and physiological consequences of HPr (ser) phosphorylation on the activities of the phosphoenolpyruvate:sugar phosphotransferase system in Gram-positive bacteria: studies with site-specific mutants of HPr. *EMBO J.* **8**, 2111–2120 (1989).
29. Napper, S. *et al.* Mutation of Serine-46 to aspartate in the histidine-containing protein of Escherichia coli mimics the inactivation by phosphorylation of Serine-46 in HPrs from gram-positive bacteria. *Biochemistry* **35**, 11260–11267 (1996).
30. Weigel, N., Kukuruzinska, M.A., Nakazawa, A., Waygood, E.B. & Roseman, S. Sugar transport by the bacterial phosphotransferase system: phosphoryl transfer reactions catalyzed by Enzyme I of *Salmonella typhimurium*. *J. Biol. Chem.* **257**, 14477–14491 (1982).
31. Garrett, D.S., Seok, Y.-J., Peterkofsky, A., Clore, G.M. & Gronenborn, A.M. Tautomeric state and pK_a of the phosphorylated active site histidine in the N-terminal domain of Enzyme I of the *Escherichia coli* phosphoenolpyruvate:sugar phosphotransferase system. *Prot. Sci.* **7**, 789–793 (1998).
32. Weigel, N., Powers, D.A. & Roseman, S. Sugar transport by the bacterial phosphotransferase system: primary structure and active site of a general phosphocarrier (HPr) from *Salmonella typhimurium*. *J. Biol. Chem.* **257**, 14499–14509 (1982).
33. Begley, G.S., Hansen, D.E., Jacobson, G.R. & Knowles, J.R. Stereochemical course of the reactions catalyzed by the bacterial phosphoenolpyruvate:glucose phosphotransferase system. *Biochemistry* **21**, 5552–5556.
34. Herzberg, O. An atomic model for protein-protein phosphoryl group transfer. *J. Biol. Chem.* **267**, 24819–24823 (1992).
35. Andersen, J.W., Pullen, J.K., Georges, F., Klevit, R.E. & Waygood, R.E. The involvement of the arginine 17 residue in the active site of the histidine-containing protein, HPr, of the phosphoenolpyruvate:sugar phosphotransferase system of *Escherichia coli*. *J. Biol. Chem.* **268**, 12325–12333 (1993).
36. Nosworthy, N.J. *et al.* Phosphorylation destabilizes the amino-terminal domain of Enzyme I of the *Escherichia coli* phosphoenolpyruvate:sugar phosphotransferase system. *Biochemistry* **37**, 65718–6726 (1998).
37. Reizer, J., Sutrina, S.L., Wu, L.-F., Deutscher, J., Reddy, P. & Saier, M.H. Functional interactions between proteins of the phosphoenolpyruvate:sugar phosphotransferase systems of *Bacillus subtilis* and *Escherichia coli*. *J. Biol. Chem.* **267**, 9158–9169 (1992).
38. Zhu, P.-P., Reizer, J. & Peterkofsky, A. Unique dicistronic operon (*ptsI-crr*) in *Mycoplasma capricolum* encoding Enzyme I and the glucose-specific Enzyme IIA of the phosphoenolpyruvate: sugar phosphotransferase system: cloning, sequencing, promoter analysis, and protein characterization. *Prot. Sci.* **3**, 2115–2128 (1994).
39. Zhu, P.-P., Reizer, J., Reizer, A. & Peterkofsky, A. Unique monocistronic operon (*ptsH*) in *Mycoplasma capricolum* encoding the phosphocarrier protein (HPr) of the phosphoenolpyruvate: sugar phosphotransferase system. *J. Biol. Chem.* **268**, 26531–26540 (1993).
40. Ottiger, M., Delaglio, F. & Bax, A. Measurement of J and dipolar couplings from simplified two-dimensional NMR spectra. *J. Magn. Reson.* **131**, 173–178 (1998).
41. Clore, G.M., Gronenborn, A.M. & Bax, A. A robust method for determining the magnitude of the fully asymmetric alignment tensor of oriented macromolecules in the absence of structural information. *J. Magn. Reson.* **133**, 216–221 (1998).
42. Clore, G.M. & Gronenborn, A.M. New methods of structure refinement for macromolecular structure determination by NMR. *Proc. Natl. Acad. Sci. USA* **95**, 5891–5898 (1998).
43. Brünger, A.T. *et al.* Crystallography and NMR system (CNS): a new software suite for macromolecular structure determination. *Acta Crystallogr. D* **54**, 901–921 (1998).
44. Koradi, R., Billeter, M. & Wüthrich, K. MOLMOL. A program for display and analysis of macromolecular structures. *J. Mol. Graphics*. **14,** 51–55 (1996).
45. Carson, M. Ribbons 4.0. *J. Appl. Crystallogr.* **24**, 958–961 (1991).
46. Laskowski, R.A., MacArthur, M.W., Moss, D.S. & Thornton, J.M. PROCHECK: a program to check the stereochemical quality of protein structures. *J. Appl. Crystallogr.* **26**, 283–291 (1993).
47. Kuszewski, J., Gronenborn, A.M. & Clore, G.M. Improving the quality of NMR and crystallographic protein structures by means of a conformational database potential derived from structure databases. *Prot. Sci.* **5**, 1067–1080 (1996).